IEEE Access
Multidisciplinary | Rapid Review | Open Access Journal

Received May 6, 2019, accepted June 6, 2019, date of publication June 10, 2019, date of current version June 25, 2019.

Digital Object Identifier 10.1109/ACCESS.2019.2922012

Smart Relay Architecture for Over-the-Horizon High Quality Communications With Unmanned Aerial Vehicles

RODRIGO BLÁZQUEZ-GARCÍA, (Student Member, IEEE), XIAOLIANG SUN, MATEO BURGOS-GARCÍA, ALEJANDRO GARCÍA-TEJERO, JUAN VIDAL-ALEGRÍA, JOSÉ-MANUEL FERNÁNDEZ-GONZÁLEZ, (Senior Member, IEEE), AND MANUEL SIERRA-CASTAÑER, (Senior Member, IEEE)

Information Processing and Telecommuncations Center, Universidad Politécnica de Madrid (UPM), 28040 Madrid, Spain

Corresponding author: Mateo Burgos-García (mateo@gmr.ssr.upm.es)

This work was supported in part by the Unmanned Solutions, S.A., in part by the Spanish National Board of Scientific and Technological Research (CICYT) under the projects FUTURE-RADIO "Radio systems and technologies for high capacity terrestrial and satellite communications in an hyperconnected world" under Grant TEC2017-85529-C3-1-R and "Communication with MIMO LTE-A/MMW transceivers for advanced services in high-mobility transportation systems" under Grant TEC2017-87061-C3-1-R, in part by the Madrid Region Government under the project "Space Debris Radar" under Grant S2013/ICE-3000. The work of R. Blázquez-García was supported by the Spanish Ministry of Education under Grant FPU15/01253. The simulations done in this work have been performed using CST Microwave Studio Suite 2016 under a cooperation agreement between Computer Simulation Technology (CST) and Universidad Politécnica de Madrid.

ABSTRACT This paper presents a system architecture to accomplish over-the-horizon communications with medium-sized unmanned aerial vehicles (UAV) in order to enhance its autonomy and maximum range. This architecture is based on using a second UAV as a communication relay with a compact active circular array with separated transmitting and receiving elements at C-band. The designed active feeding network provides switching capabilities in order to selectively activate these elements depending on the desired direction of the antenna beam, achieving maximum equivalent isotropic radiated power (EIRP) in transmission and maximum antenna gain in reception. In this way, a bidirectional long-range link for telemetry, telecommand, and high-resolution video can be deployed between UAVs providing high quality of service, reliability, and moderate data throughput at an affordable cost. Based on the measurements of a manufactured prototype, the maximum range of the deployed air–air link using the designed system is estimated in 20 km, considerably increasing the performance of current systems based on the use of omnidirectional antennas onboard UAVs.

INDEX TERMS Antenna array, beam steering, beam-switching, microwave circuits, over-the-horizon communications, patch antennas, relay architecture, switched circuit, unmanned aerial vehicle (UAV).

I. INTRODUCTION

Unmanned aerial vehicles (UAV) are being increasingly used in applications such as remote sensing [1], disaster-management [2] and enhanced situational awareness for military mission planning [3] thanks to their higher flexibility and cost-effectiveness than piloted aircraft. The stand-off control and autonomy of these vehicles is specially useful to monitor difficult access areas where the safety of the pilot can be compromised. However, the autonomy of UAVs is currently limited by the maximum range of the communication links used for sending telecommands and the data captured by the airborne sensors. These links are usually deployed at S, C or K band and they require a line of sight between the base station and the mission UAV. Therefore, the maximum range of these links are highly dependent on the terrain orography.

In order to overcome this problem, the usage of satellite connections such as Iridium system or geosynchronous satellites has been suggested [4], [5], but they require complex, heavy and expensive beam tracking systems, including joint mechanical and electrical adjustments [6], or they suffer from communication outages or insufficient data throughput [7]. Consequently, this is not considered a cost-effective and reliable solution for over-the-horizon (OTH) communication with small and medium-sized UAVs.

The associate editor coordinating the review of this manuscript and approving it for publication was Wenjie Feng.

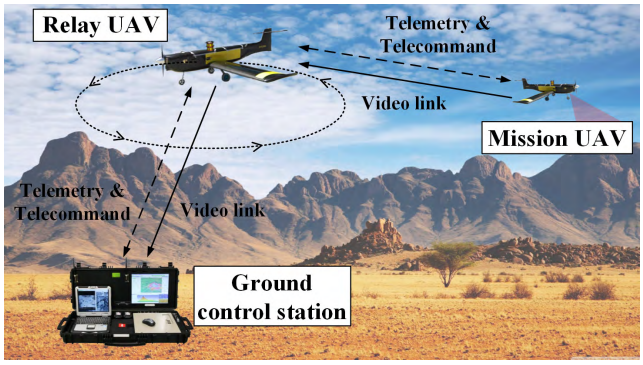

FIGURE 1. Over-the-horizon UAV-relay system for long range dual channel communication (bidirectional telemetry and telecommand and downlink high bandwidth video). The relay and mission UAVs maintain a line-of-sight link using the proposed electronic steerable antenna system.

In this paper, a long-range OTH communication system for UAVs with high quality of service, moderate data throughput and affordable cost is proposed based on the use of a second UAV as a communication relay, as shown in Fig. 1. This relay UAV should fly close to the ground station in order to guarantee line-of-sight connectivity, but at a sufficient altitude to avoid terrain obstacles that could block the air-air link between the relay UAV and the mission UAV. Besides, this communication system provides bidirectional coverage for telemetry and telecommand, and a high-capacity downlink for high-resolution video or equivalent payload sensors.

Several works have analysed the use of UAVs as communication relays in order to extend the coverage area and operational range of the mission UAV and increase data throughput [8]–[10], showing the great potential of this system architecture. In [11], the usage of directional antennas mounted on rotating platforms with heading control is proposed in order to increase the communication range of this relay architecture.

The key point of this paper is the design and manufacturing of a communication system at C band (5 GHz), including both the RF front end and the antenna system, which can be mounted onboard medium-sized UAVs to provide this relay capability using highly reliable electronically steerable antennas. In this way, the increased antenna gain allows to achieve a longer maximum range and greater flight autonomy for UAVs than current communication systems, without the need of mechanical scanning devices.

Our proposed system is based on a compact active circular array with separated transmitting and receiving elements at C band and it can be installed onboard medium-sized UAVs for air-air links. In addition, it can be steered over the whole 360° azimuth range depending on the relative position between the relay and mission UAVs in order to obtain maximum equivalent isotropic radiated power (EIRP) in transmission and maximum antenna gain in reception, improving the performance of those systems based on the use of omnidirectional antennas.

The application of smart antennas and phased-arrays with tracking systems for ground stations has been developed during the last few years [12], [13], and they are in operation for medium and large-sized UAV communication systems. In this regard, the usage of distributed access points with multiple antennas, exploiting both space diversity and array gain, has been proposed in [14] to provide ultra-reliable and low-latency communications between ground stations and UAVs. However, there hardly exists any similar system for airborne platforms.

H. C. Nguyen et al. [15] analysed different techniques that improve the throughput and reliability of the UAV connectivity over cellular networks. Among these techniques is the antenna beam selection technique, which can be implemented by the use of conformal arrays mounted on the UAVs with beam switching capabilities.

Conformal arrays with beam switching capabilities based on passive feeding networks have been presented in [16] and [17]. Jaeck et al. [16] developed a conical antenna at C band made of four switched 3-element subarrays spaced by 90° in the azimuth plane with beam steering capabilities in the elevation plane. In this case, a complex control system is required to apply the suitable driving signals to the phase shifters of the beamforming network. Sanchez-Olivares et al. [17] presented a compact eight-element circularly conformal array antenna at S band, but its feeding network only allows four switched beams of 90° angular separation in azimuth. This low angular resolution entails approximately a 10 dB antenna gain loss at the boundaries of the sector covered by each switched beam.

Taking into account compactness, manufacturing cost and control complexity as design criteria, our conformal circular antenna array is based on the same compact geometry as [17], implementing an eight-faced regular prism, but our developed feeding network allows a more flexible activation of the antenna elements and an angular resolution of 45° between switched beams, limiting the antenna gain loss to 3 dB at the boundaries of each sector. In order to extend the maximum communication range of the system, our feeding network includes active transmitting and receiving paths, increasing the EIRP in transmission and enhancing the noise figure in reception. Besides, the use of separated transmitting and receiving elements improves the isolation between transmitting and receiving paths, allowing the frequency-division duplex (FDD) operation.

This paper is organized as follows. Section II presents the architecture of the system and its different modules. In Section III, the design of the circular antenna array is explained, and the measurements performed of the manufactured prototype are shown. The design and prototyping of the RF front end to provide beam switching capabilities, including the transmitting and receiving branches, and the performance estimation of the integrated system based on measurements are presented in Section IV. Finally, concluding remarks are drawn in Section V.

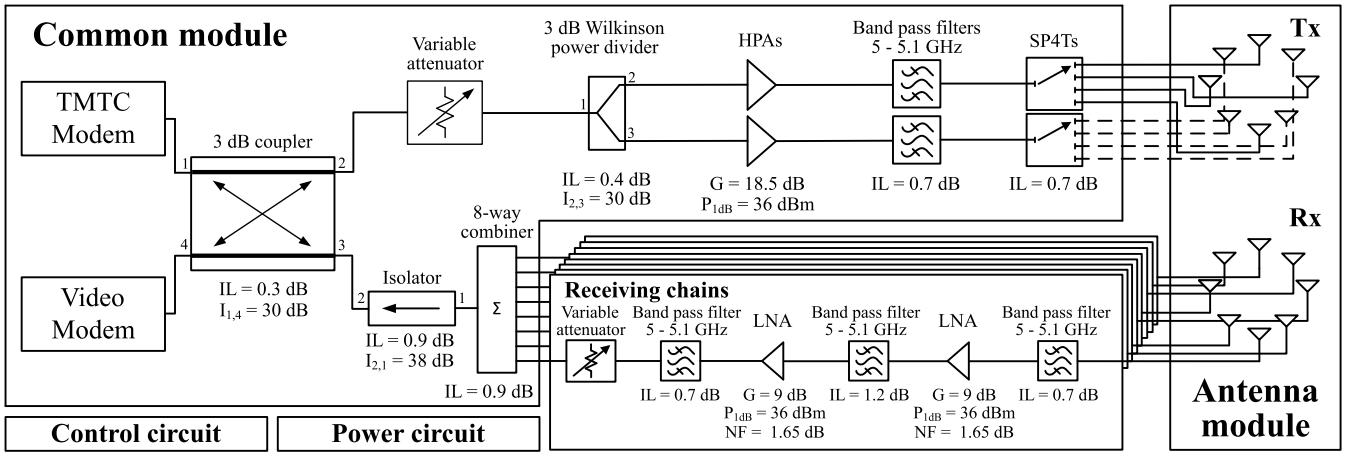

FIGURE 2. System architecture divided into: a common module with a dual modem configuration (Telemetry and telecommand -TMTC- modem and video modem) and active transmitting feeding paths, receiving modules for each antenna receiving element, control circuit, power circuit, and antenna system based on two separated circular arrays for transmission and reception with eight patches each. Single-pole, four throw (SP4T) switches are connected to the transmitting antenna elements in a way that allows to activate simultaneously two adjacent elements. (Notation: IL = Insertion loss; $I_{n,m}$ = Isolation from port *n* to port *m*; G = Power gain; P_{1dB} = 1 dB compression point; NF = Noise figure).

II. SYSTEM ARCHITECTURE

The frequency band designated for the system is the C band, particularly from 5030 to 5091 MHz, which is allocated for UAV control and non-payload communications (CNPC) [18].

As shown in Fig. 2, our system consists of the following modules: a common module that includes both modems for Telemetry and Telecommand (TMTC) and video transmission (dual modem configuration), the transmitting branch and the common receiving branch up to the eight-way power divider; the receiving modules for each antenna element which can be activated depending on the desired beam direction; the control module that selectively activates each radiating element by commanding the switches and the enable circuits of the power amplifiers; the power module that provides energy supply to each active device, and the antenna system composed of two eight-element circular arrays for separated transmission and reception. In this way, an active and electronically steerable array is implemented in order to increase the antenna gain and, therefore, the maximum range of the mission UAV in comparison with the usage of omnidirectional antennas.

This proposed system allows the implementation of beam-switching techniques to cover the whole 360° azimuth range using directional antennas. In this way, as shown in Fig. 3, the antenna beam direction can be controlled by selectively activating different radiating elements depending on the relative position between UAVs.

Including phase shifters in the RF front-end would additionally allow to steer the beam continuously in each sector, reducing the antenna gain loss at its boundaries and making the use of radiating elements with higher directivities possible, at the expense of a higher control complexity. In this case, the application of a phased array would require a more accurate positioning and tracking system of both UAVs with a fast update rate due to the agile dynamics of these aerial

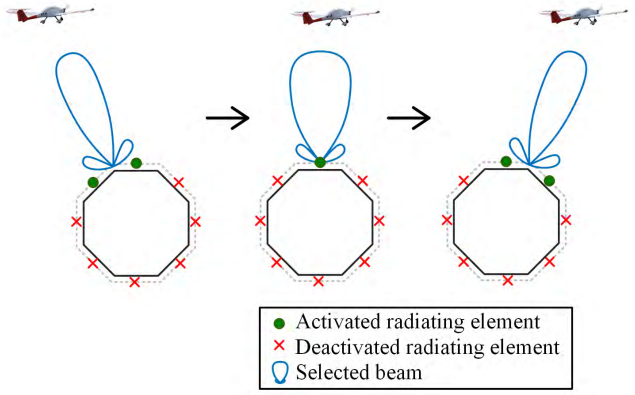

FIGURE 3. Example of a beam-switching scheme to select the desire beam direction depending on the relative position between UAVs.

platforms. However, these antenna modules would not meet our requirements of compactness and low control complexity to be mounted on medium-sized UAVs. For this reason, we considered beam switching as a compromised solution to provide higher directivities than omnidirectional antennas but with a control system of low complexity. Taking this into account and the required compactness, we designed our RF front-end, radiating elements and array geometry to provide certain directivity while limiting the antenna gain loss at the boundaries of the beam-switching sectors.

A. COMMON MODULE

The common module includes two modems: one for TMTC transmission [19], and the other for high resolution video transmission [20]. These modems are multiplexed in frequency in order to be able to work simultaneously without interfering each other since they share the same transmission and reception paths. In turn, each modem employs

time-division duplexing (TDD) to separate transmission and reception, but the developed system can also work with FDD modems.

The control information sent by the TMTC modem using Gaussian minimum-shift keying (GMSK) modulation includes telemetry, telecommands, location and system information and it requires a reliable and robust bidirectional link with narrow bandwidth. On the other hand, the video captured by the mission UAV is streamed by the video modem using coded orthogonal frequency division multiplexing (COFDM) modulation with adaptive modulation and coding (AMC) scheme based on the signal-to-noise ratio (SNR) of the link. This video information requires a bidirectional link but quite asymmetrical. The overall bandwidth available for both links is 61 MHz in the designated frequency band.

The modem signals go to a 3 dB coupler, which is connected to the transmission and reception branches. This coupler should have a relatively high isolation and return losses in order to avoid high incident power in the modems due to reflections and crosstalk, which could affect their performance. In the transmission branch, there is a variable attenuator in order to adapt the output transmitted power of the modems to the required level. Then, the transmission feeding network is composed of a 3 dB Wilkinson power divider that separates the branch into two paths in which the signal is amplified by high power amplifiers (HPA) and filter to limit the transmitted bandwidth according to regulation. Finally, each path is connected to a single-pole, four throw (SP4T) switch, which allows to select one out of the four connected antenna patches of the eight-element circular transmitting array. In this way, the system selectively transmits through two adjacent antenna elements achieving an electronically steerable radiation pattern as will be discussed in the following sections.

In the reception branch of the common module, the receiving modules are connected to an 8-way power combiner. In this case, as well as activating two adjacent antenna elements, it is also possible to select only one antenna element to receive because the receiving modules can be disabled. This will let the system to define the beam direction of the receiving radiation pattern. Finally, to protect the components of the reception branch, an isolator is connected between the power divider and the 3 dB coupler.

B. RECEIVING MODULES

Each antenna element of the receiving circular array is connected to a receiving module which is essentially an amplification and narrowband-filtering stage to adapt the received signal to the power requirements and eliminate interfering bands. In these receiving modules, as shown in Fig. 2, firstly, a band-pass filter removes the non-desirable frequency components of the signal received by the antenna. Secondly, a low noise amplifier (LNA) increases the power of the signal and avoids degradation of the noise factor of the system. This is followed by another band-pass filter and a second amplification stage with a high P1dB in order to avoid saturation of the receiving chain. Finally, the signal is band-pass filtered again and a variable π attenuator can regulate the chain gain to provide the module with a certain level of freedom.

C. ANTENNA SYSTEM AND CONTROL AND POWER MODULES

The antenna system is based on two eight-element circular arrays, one for reception and the other for transmission, in order to guarantee a good isolation between transmitting and receiving channels. Each array consists of eight circular patches, although only two patches are activated simultaneously for transmission and one or two for reception. Thus, their beam direction can be electronically steered depending on the relative angle between the mission UAV and the relay UAV. Each patch antenna of the transmitting array is connected directly to an output on one SP4T switch by a coaxial cable and SubMiniature version A (SMA) connectors in order to reduce the losses. On the other hand, each element of the receiving array is connected to a receiving module mounted on the rear side of the ground plane of the antenna.

The control module consists of a microcontroller that decides which patches are activated depending on the second UAV position and the measured received power, following an adaptive switching scheme.

Finally, the power module provides energy supply to each active device. Since the voltage supply is provided by the UAV battery, which is a noisy source, this module filters and regulates the power.

III. ANTENNA SYSTEM DESIGN

The antenna system consists of a double circular array of eight elements with separated transmission and reception, whose preliminary design was described in [21]. As said before, these elements are selectively activated depending on the desired beam direction. Thanks to the designed feeding network, in transmission, two adjacent elements can be activated in order to obtain maximum equivalent isotropic radiated power (EIRP), whereas in reception, one or two adjacent elements can be selected in order to obtain maximum antenna gain. Switching the activated receiving and transmitting elements allows to define the beam pointing of the directional antenna, which is the main characteristic of this system to enhance the maximum range of the mission UAV in beyond line-of-sight (BLOS) or over-the-horizon (OTH) situations.

A. ANTENNA ELEMENT

The antenna element, which operates at a center frequency of 5.0605 GHz, consists of two microstrip circular patches with vertical polarization for separated transmission and reception, as shown in Fig. 3. The specifications of this element are shown in Table 1. The selection of a patch antenna as the radiating element has been made regarding its small size, low profile, simple geometry and low cost. The preliminary design of the radiating element to work at 5.065 GHz based on [22] has been optimized to reduce the return loss in the

TABLE 1. Specification of the antenna element.

Parameter	*Specification*	*Units*
Working band	5.03 to 5.091	GHz
Polarization	Vertical	-
Maximum gain	> 6	dBi
3 dB beamwidth in elevation	> 50	degrees

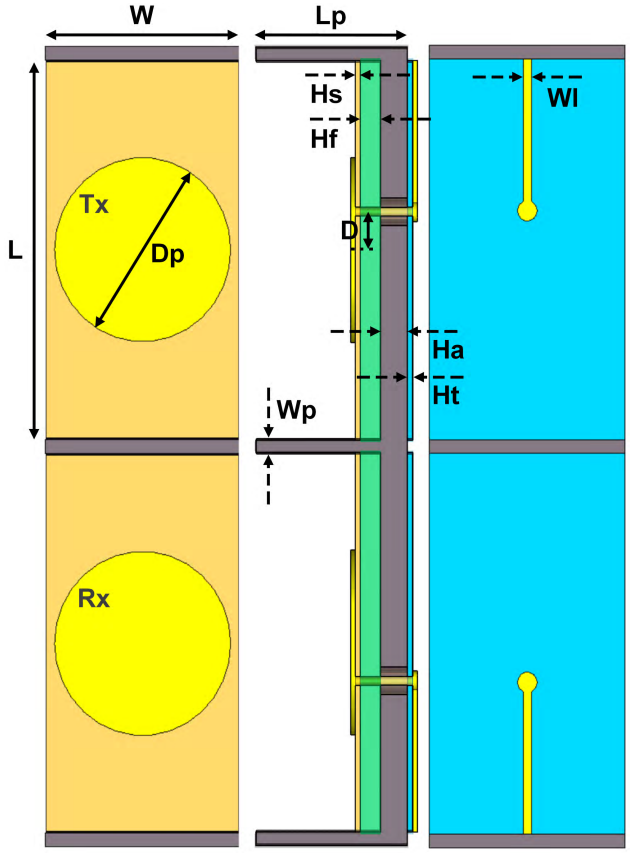

FIGURE 4. Geometry and layer structure of the proposed antenna element based on two circular patches for separated transmission and reception.

operating bandwidth (5.03-5.091 GHz) using Computer Simulation Technology (CST) software and considering standard manufacturing thicknesses for the different layers.

Each radiating element consists of one circular patch with a radius (Dp/2) of 13.7 mm, a coaxial to microstrip transition stacked between three substrate layers and a rectangular ground plane. The length (L) and width (W) of the substrates and the ground plane is 58×30 mm. Fig. 3 also shows the distribution of the different layers. The top layer, where the patch is placed, corresponds to a 0.254 mm-thick (Hs) FR-4 substrate (dielectric constant $\varepsilon_r = 4.3$ and loss tangent $\tan\delta = 0.025$ at 10 GHz) with a 35 μm copper metallization for the patch. This layer is followed by a 3 mm-thick (Hf) foam sheet and a 4 mm-thick (Ha) aluminium ground plane. At the back of the ground plane, an SMA connector or the printed circuit board (PCB) of the receiving module will be placed for the transmitting and receiving elements, respectively.

TABLE 2. Dimensions of the antenna element defined in Fig. 4 and optimized by CST software, considering standard manufacturing thicknesses for the different layers, to minimize the return loss in the operating bandwidth (5.03-5.091 GHz), adjust the 3 dB elevation beamwidth to 50° and improve the isolation between transmitting and receiving elements.

Parameter	*Value*	*Parameter*	*Value*
L	58 mm	Ha	4 mm
W	30 mm	Ht	0.508 mm
Dp	27.4 mm	D	5.7 mm
Lp	20.5 mm	Wp	2 mm
Hs	0.254 mm	Wl	1.3 mm
Hf	3 mm		

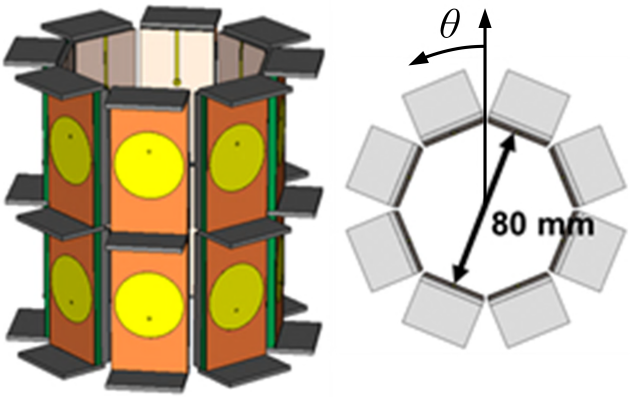

FIGURE 5. 3D and top views of the designed antenna array composed of two circular arrays of eight radiating elements. The top array is used for transmission, while the bottom array is used for simultaneous reception.

However, for the design, manufacturing and measurement of the antenna element prototype, a 0.508 mm-thick (Ht) TLY-5A Taconic substrate ($\varepsilon_r = 2.17$ and $\tan\delta = 0.0009$ at 10 GHz) with a 35 μm copper metallization will be used instead of the receiving module. In this layer, a microstrip line is placed to feed the antenna.

The feeding of the circular patch is located at a distance (D) of 5.7 mm from the center. At this point, the patch is soldered to the conductor of a coaxial cable, which connects it with the feeding microstrip line of the antenna element prototype. Furthermore, planes of aluminium are situated at the top and bottom sides of each patch antenna to reduce the electromagnetic interference from the rest of the array, improve isolation between receiving and transmitting arrays, adjust the 3 dB elevation beamwidth to 50° and increase antenna directivity. These planes have a length (Lp) of 20.5 mm. Table 2 summarizes the dimensions of the antenna element.

B. ANTENNA ARRAY PROTOTYPE AND MEASUREMENTS

The designed antenna array structure is shown in Fig. 5. This antenna system is composed of two circular array of eight radiating elements. The top array is used as the transmitting antenna, where two adjacent radiating elements are activated simultaneously depending on the desired beam direction.

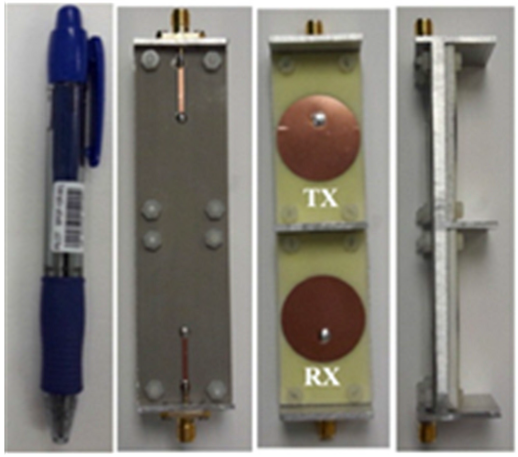

FIGURE 6. Front, rear and side views of the manufactured prototype of an array element with both transmitting and receiving patches.

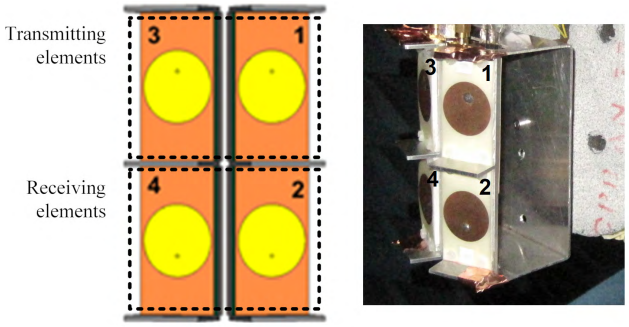

FIGURE 7. Geometry of a 2 × 2 element configuration for transmission and reception, and measurement setup in the anechoic chamber of Universidad Politécnica de Madrid.

The bottom array is used for simultaneous reception and, in this case, one or two adjacent radiating elements are activated in order to obtain the maximum receiving antenna gain in the direction of the mission UAV. The transmitting and receiving antennas are separated by aluminium material in order to improve isolation.

Fig. 6 shows the manufactured prototype of an array element with both transmitting and receiving patches. Considering the geometry of a 2 × 2 element configuration including both transmitting and receiving antennas, as shown in Fig. 7, the simulated and measured S-parameters with respect to element 1 are represented in Fig. 8. The measured reflection coefficient response has been shifted in comparison with the simulated result in CST because a 0.2 mm-thick substrate was used for the manufactured prototype instead of the 0.254 mm-thick substrate used in simulations. Nevertheless, a return loss higher than 20 dB is still obtained for each element in the considered operating bandwidth. Besides, the measured isolation between transmitting and receiving elements is above 35 dB, whereas the isolation between adjacent transmitting or receiving elements is about 30 dB.

Fig. 9 shows the simulated and measured radiation patterns at 5.0605 GHz and Fig. 10 shows the maximum antenna

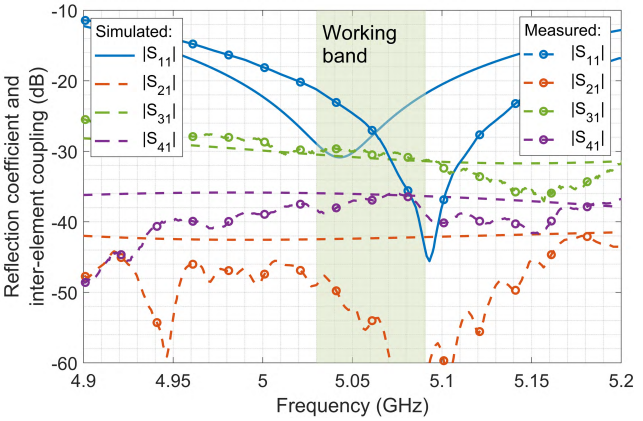

FIGURE 8. Simulated and measured reflection coefficient (solid lines) and inter-element couplings (dashed lines) for the 2 × 2 element configuration with respect to element 1.

gain in the beam direction as a function of frequency when activating one or two adjacent radiating elements of the considered configuration. In general, measurements show good agreement with simulations, achieving a maximum antenna gain of about 10 dB in the operating band when activating two adjacent elements or 8.4 dB when activating a single element. However, the radiation pattern of element 3 exhibits a 1 dB loss in its maximum gain with respect to simulation possibly due to manufacturing inaccuracies of this radiating element since this decline is not shown in the radiation pattern of element 1. The measured half power beamwidth (HPBW) obtained in the horizontal plane for the considered configuration is 87° and 49° when activating, respectively, one or two adjacent radiating elements. Regarding the vertical plane, the measured HPBW is above 50° for the considered situations. Therefore, the presented measurements of the manufactured prototype meet the requirements of the antenna system.

IV. RF FRONT END

Besides the antenna system, the RF front end is one of the key parts of our proposed design because it connects the data modems with the antennas and includes the switching network that controls which antenna elements are activated depending on the desired beam direction. As shown before in the system architecture (Fig. 2), the RF front end is divided into a common module and several receiving chains, whose design and measurements results are presented in this section.

A. DESIGN

The main specifications of the RF front end are summarized in Table 3. The receiving chain should provide enough amplification gain in order to avoid the decline of the SNR due to the noise generated by the UAV engines in the modems, whose power is independent of this amplification gain. Therefore, a minimum gain of 10 dB is required in each receiving chain to guarantee that antenna and thermal noise are higher than engine noise. The isolation between transmitting and receiving chains in order to avoid the saturation of the

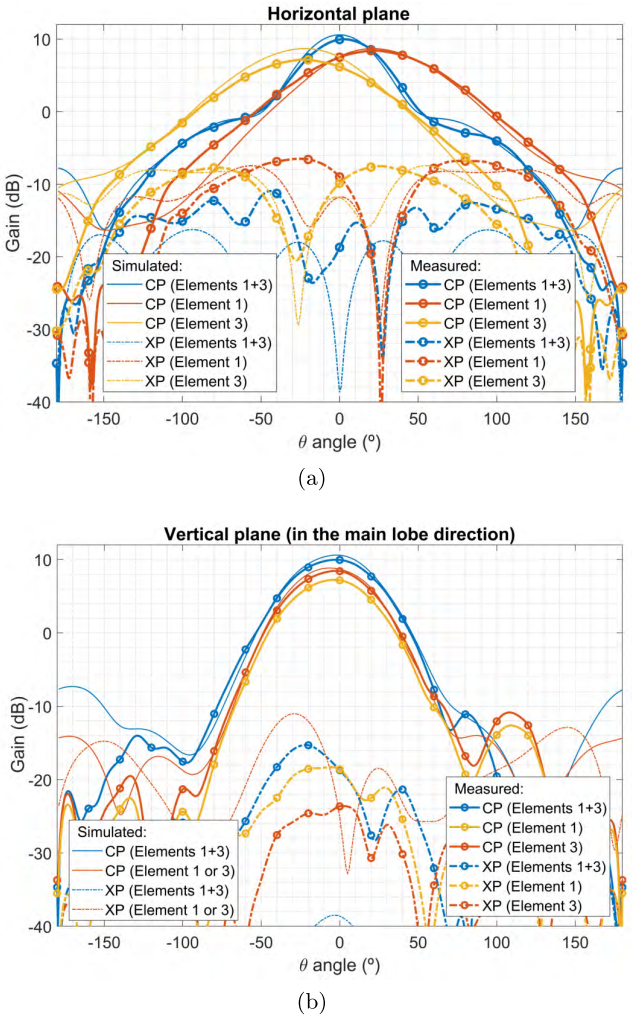

FIGURE 9. Simulated and measured co-polarization (CP, solid lines) and cross-polarization (XP, dashed lines) components at 5.0605 GHz when radiating through two adjacent elements (1 and 3) or only one element (1 or 3): (a) Horizontal plane and (b) Vertical planes (in the main lobe direction of each radiation pattern).

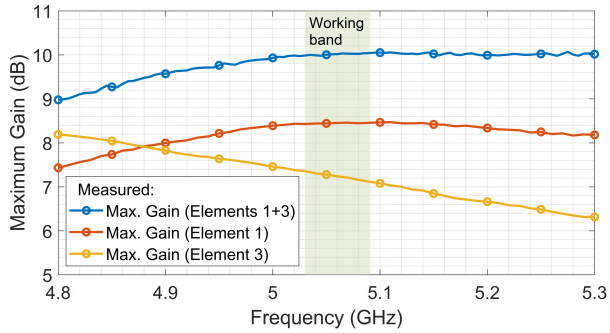

FIGURE 10. Maximum antenna gain measured in the beam direction as a function of frequency when radiating through two adjacent elements (1 and 3) or only one element (1 or 3).

receiving chain amplifiers should be higher than 35 dB. This value is achieved by the isolation between transmitting and receiving antenna elements, as shown in the measurements of the manufactured antenna presented in the previous section.

TABLE 3. Specification of the RF front end.

Parameter	*Specification*	*Units*
System bandwidth	80	MHz
Noise factor	< 4	dB
Receiving chain gain	> 15	dB
Transmission chain output power	> 34	dBm
Tx-Rx isolation	> 35	dB

Based on the block diagram shown in Fig. 2, the common module, which includes a transmitting branch with active switching capabilities and a receiving branch that combines the output of the eight receiving chains, is assembled in a single PCB. The modems transmit an output power above 28 dBm. The 3 dB coupler which separates the transmitting and receiving branches has an isolation of about 30 dB and an insertion loss of 0.3 dB.

Regarding the transmission branch, the variable attenuator allows to adjust the transmitting power to avoid saturation. The Wilkinson divider has an isolation of 30 dB and an insertion loss of 0.4 dB. The power amplifiers have a gain of 18.5 dB and an output 1 dB compression point (P1dB) of 36 dBm, whereas the filters have a narrow band from 5 to 5.1 GHz with an insertion loss of 0.7 dB. Finally, the SP4T switches have an insertion loss of 0.7 dB and they allow to activate the two adjacent radiating elements that achieve the maximum EIRP in the direction of the mission UAV. In this way, the output power of each transmission chain is above 34 dBm, achieving a maximum EIRP of about 47 dBm in the direction of the beam when combining two adjacent active elements.

In the receiving branch, the eight-way combiner has an insertion loss of 0.9 dB. Besides, the isolator has an insertion loss of 0.9 dB, an isolation of 38 dB from output port to input port and a maximum incident power in the output port of 37 dBm.

Each receiving chain is assembled on the rear part of each array element using grounded coplanar waveguide technology. Both low noise amplifiers have a gain of 9 dB, a P1dB of 24 dBm and a noise factor of 1.65 dB. The filters have a narrow band from 5 GHz to 5.1 GHz in order to avoid interferences from other bands and they have an insertion loss of 0.7 dB, 1.2 dB and 0.7 dB, respectively. Finally, the attenuator, whose attenuation should be lower than 5 dB, allows to adjust the received power level to a suitable value. In this way, a total gain of the receiving chain higher than 10 dB is guaranteed. Besides, the noise factor of the receiver branch is 3.5 dB.

B. RECEIVING CHAIN PROTOTYPE AND MEASUREMENTS

Fig. 11 shows a manufactured receiving chain with a 4 dB π attenuator assembled on the rear part of an array element. The measured S-parameters of this receiving chain, considering the input (antenna port) as port 1 and the output as port 2,

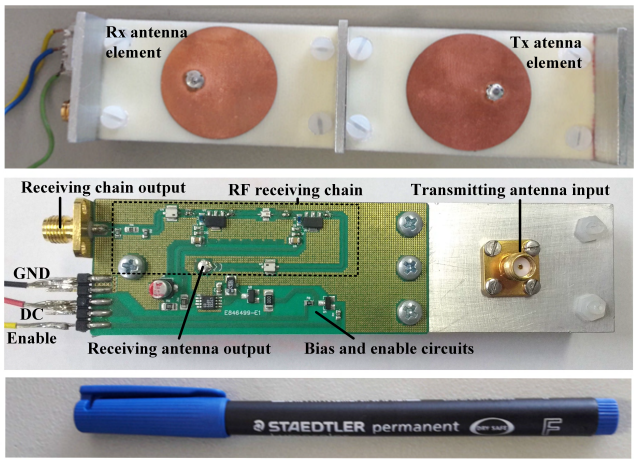

FIGURE 11. Front and rear part of a manufactured array element with the receiving chain assembled.

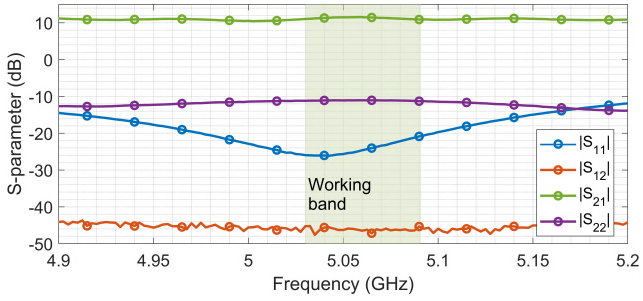

FIGURE 12. Measured S-parameters of the manufactured receiving chain with a 4 dB π attenuator considering the input (antenna port) as port 1 and the output as port 2.

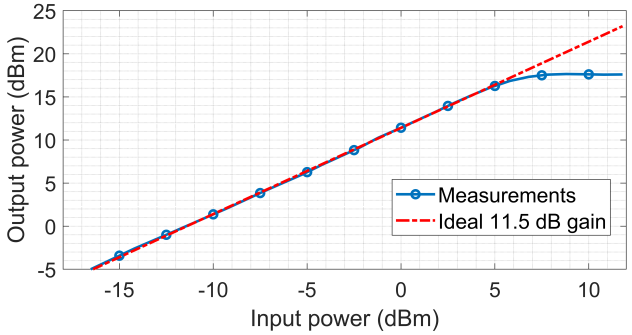

FIGURE 13. Measured output power of the manufactured receiving chain as a function of the input power at 5.0605 GHz.

are represented in Fig. 12. The reflection coefficient is below -20 dB and the total gain is 11.5 dB with a 0.6 dB ripple in the operating band. These values are in agreement with the specifications of the components.

Fig. 13 shows the output power of the receiving chain as a function of the input power at 5.0605 GHz in order to analyse its saturation. The 1 dB compression point is reached at an input power level of 6.8 dBm achieving an output power of 17.3 dBm. According to the specifications of the LNAs and taking into account the attenuation after the second LNA of the receiving chain, this value is 2 dB lower than

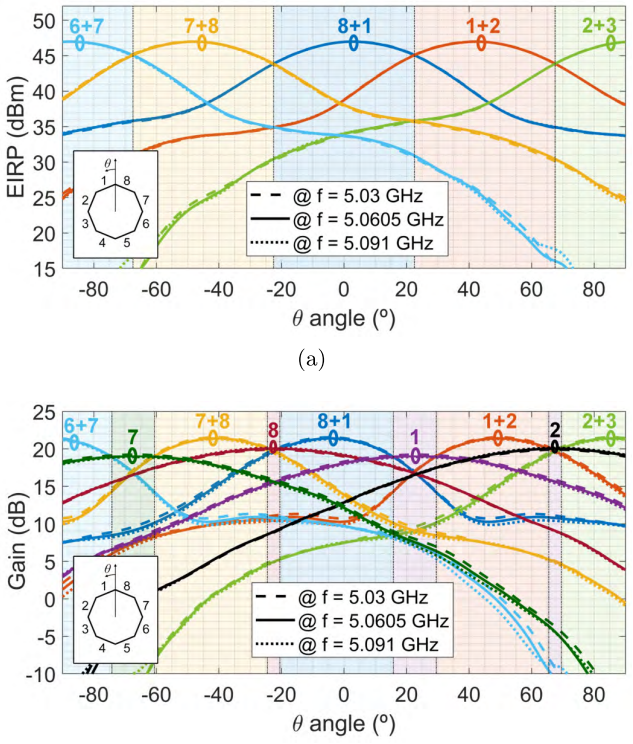

FIGURE 14. Transmitting and receiving switched beams in the horizontal plane at the center and limit frequencies of the operating bandwidth for the −90° to 90° azimuth range inferred from the measurements of a 2 × 2 configuration integrating the antenna and the RF front end: (a) EIRP at 1 dB compression point (transmission) and (b) Total gain in reception at the output of the combiner including antenna and receiving chains.

the expected, possibly due to the actual performance of the LNAs. However, the response is highly linear, which is an important characteristic in order to avoid the distortion of the signal when using non-constant envelope modulation as orthogonal frequency division multiplexing (OFDM).

C. SYSTEM INTEGRATION AND PERFORMANCE ESTIMATION

In order to characterize the performance of the proposed design, a prototype including two transmitting and receiving elements with the corresponding active feeding network was manufactured. This prototype was measured in the anechoic chamber (measurement setup similar to Fig. 7) to determine its achieved EIRP and receiving gain. Based on the measurements of this 2 × 2 configuration in which the RF front end and the antenna are integrated, the switched beams in transmission and reception of the whole circular active array can be approximately inferred. Small discrepancies are expected with respect to the actual beams due to manufacturing differences between radiating elements. Fig. 14a shows the EIRP at 1 dB compression point in the horizontal plane of the different beams formed by activating two adjacent transmitting elements. Each beam covers a 45° sector, achieving a maximum EIRP at 1 dB compression point of 47 dBm and a minimum EIRP of 43.9 dBm in the covered sector.

The total gain in the horizontal plane at the output of the combiner of the receiving chains including the antenna for the different beams formed by activating one or two adjacent receiving elements is represented in Fig. 14b. Depending on the relative position of the UAVs, the maximum receiving gain is achieved by activating one or two adjacent elements. Based on this switching scheme, considering the whole 360° azimuth range in the horizontal plane, the maximum and minimum receiving gains are 21.4 dB and 18.9 dB, respectively. Besides, the radiation patterns of the switched beams hardly change along the considered operating bandwidth.

The control module of the system selects which elements are activated by commanding the SP4T switches and the enable circuits of the amplifiers based on Global Positioning System (GPS) measurements of both UAVs or scanning the beams to determine which one achieves the highest received signal strength indicator (RSSI) provided by the modems.

Using the software control tool of the video modems which allows to estimate the signal-to-noise ratio (SNR) of a received signal, link measurements in lab conditions were performed by using attenuators to simulate the link attenuation between the transmitting and receiving chains of two separated modems. In this way, we were able to confirm that the video modems can work with the SNR specified in the Digital Video Broadcasting-Terrestrial (DVB-T) standard for video transmission [23]. In this measurement, the required 10 dB SNR for the GMSK modulation of the telemetry and telecommand link was also verified. Therefore, the maximum range of the link can be estimated by using these required SNR and assuming a Gaussian channel, which is suitable for open environments typical of the considered UAV operation [24].

Taking into account the measurements of the manufactured prototype and the specifications of the modems, the performance of the relay system has been estimated for a transmission channel of 8 MHz based on the following power budget expression to estimate the SNR of the link:

$$\begin{aligned} SNR\,[\mathrm{dB}] = {} & EIRP\,[\mathrm{dBm}] - OBO\,[\mathrm{dB}] + G_{RX}\,[\mathrm{dB}] \\ & - L_p\,[\mathrm{dB}] - (-174\,\mathrm{dBm/Hz} \\ & + 10\log_{10}(B\,[\mathrm{Hz}]) + F\,[\mathrm{dB}]), \end{aligned} \tag{1}$$

where OBO is the output back-off, G_{RX} is the receiving antenna gain, L_p is the propagation loss, B is the channel bandwidth, and F is the system noise figure.

Table 4 shows the results of the performed power budget for a link range of 20 km. Given the use of OFDM modulation and simple peak-to-average power ratio (PAPR) reduction techniques such as peak windowing implemented in the modem operation, an output back-off of 5 dB is considered to avoid saturation of the transmitting chains [25]. The transmission losses at 5.1 GHz were computed using the IF77 propagation model following ITU Recommendation ITU-R P.528-3 [26] and ITU Report ITU-R P.2345-0 [27] for an availability of 95% and an altitude of 1000 m for both UAVs. Based on the use of Digital Video Broadcasting-Terrestrial (DVB-T) standard for video transmission, the required SNR is 3.5 dB [23] for a modulation and coding scheme (MCS) with quadrature phase-shift keying (QPSK) constellation and inner code rate of 1/2 considering a non-hierarchical transmission and a Gaussian channel [24]. This MCS achieves a useful bitrate of 5.53 Mbps for a guard interval to useful symbol time ratio of 1/8, which is enough for compressed high-resolution video transmission. In this way, a link margin of 6.75 dB is achieved, which is suitable to compensate the decrease in EIRP and receiving antenna gain due to the radiation pattern and the actual relative position between UAVs, the polarization mismatch losses and possible inaccuracies of the propagation model. Besides, the use of AMC and the calculated link margin allow to obtain higher data throughput in favorable situations.

TABLE 4. Power budget for a 20 km-long video link.

Parameter	*Value*
Maximum EIRP at 1 dB compression point	47 dBm
Output back-off	5 dB
Maximum receiving antenna gain	10 dB
Transmission losses (20 km, 95% availability) IF77 model	143.2 dB
System noise figure	3.5 dB
Channel bandwidth	8 MHz
Estimated SNR	10.25 dB
Required SNR for QPSK and 1/2 code rate	3.5 dB
Link margin	6.75 dB

On the other hand, the telemetry and telecommand link transmits a 100 kHz-bandwidth GMSK modulation which requires a SNR of 10 dB. In this case, the estimated maximum range is above 100 km for an availability of 95%. Consequently, this control link does not limit the autonomy of the mission UAV and shows a great reliability even in demanding situations when outages of the video link may occur. In fact, considering a 20 km-link and an availability of 99%, this control link has an additional link margin of 12 dB based on the IF77 propagation model. It is also important to note that the proposed hardware architecture with low-control complexity does not degrade the latency of the link, which is mainly determined by the selected relay modems and communication protocols [7]. These protocols can be optimized in UAV relay systems [28] to enable low-latency communications, which are required for UAV control links.

Therefore, thanks to the increased EIRP and receiving gain, the proposed relay system achieves an estimated maximum range of 20 km for high-resolution video transmission, enhancing the autonomy and the operational range of the mission UAV independently of the terrain orography, and maintains a high robustness of the control link. This estimation will be verified in field tests with the actual operational conditions.

TABLE 5. Comparison of steerable directional antennas for UAV-UAV communications.

	Our work	Sanchez-Olivares et al. [17]	Jaeck et al. [16]	Chen et al. [11]
Size (mm)	80x80x122	127x127x52	52x52x95	31x80x161
Frequency of operation	C band (5.06 GHz)	S band (3.5 GHz)	C band (5.2 GHz)	S band (2.4 GHz)
Employed technique	Beam switching	Beam switching	Beam switching (azimuth) / phased array (elevation)	Mechanical steering
Angular resolution	45°	90°	90° (azimuth) / Almost continuous (elevation)	Almost continuous
Control complexity	Low	Low	Medium	High
Max. EIRP	47 dBm	16 dBm	Not specified	28 dBm
Max. receiving antenna gain	10 dBi	8 dBi	10 dBi	8dBi

Table 5 shows a comparison between our work and recently published designs of steerable directional antennas with 360° coverage which can be employed for UAV-UAV communications. Our proposed design presents improvements in terms of EIRP and beam-switching angular resolution while maintaining a compact size, a low manufacturing cost and a low control complexity.

V. CONCLUSION

In this paper, a UAV communication system at C band has been proposed based on a circular active array antenna with beam switching capability to deploy air-air links and extend the autonomy of current medium-sized UAVs by using a second UAV as a relay. This compact system provides a reliable bidirectional link for telemetry, telecommands and high-resolution video at an affordable cost. The antenna module consists of two circular arrays for separated transmission and reception with eight elements which are selectively activated to achieve maximum EIRP and maximum receiving antenna gain in the desired direction. Based on the experimental characterization of a manufactured prototype, a maximum range of 20 km has been estimated for a 8 MHz transmission channel with 5.53 Mbps useful bitrate, enhancing the performance of current systems based on the use of omnidirectional antennas onboard UAVs.

REFERENCES

[1] I. Colomina and P. Molina, "Unmanned aerial systems for photogrammetry and remote sensing: A review," *ISPRS J. Photogram. Remote Sens.*, vol. 92, pp. 79–97, Jun. 2014. doi: 10.1016/j.isprsjprs.2014.02.013.

[2] M. Erdelj, E. Natalizio, K. R. Chowdhury, and I. F. Akyildiz, "Help from the sky: Leveraging UAVs for disaster management," *IEEE Pervasive Comput.*, vol. 16, no. 1, pp. 24–32, Jan. 2017. doi: 10.1109/MPRV.2017.11.

[3] R. P. Higgins, "Automatic event recognition for enhanced situational awareness in UAV video," in *Proc. IEEE Military Commun. Conf.*, Atlantic City, NJ, USA, Oct. 2005, pp. 1706–1711.

[4] A. J. Mohammad, V. Frost, S. Zaghloul, G. Prescott, and D. Braaten, "Multi-channel Iridium communication system for polar field experiments," in *Proc. Int. Geosci. Remote Sens. Symp. (IGARSS)*, Anchorage, AK, USA, Sep. 2004, pp. 121–124.

[5] J. Zhao, F. Gao, Q. Wu, S. Jin, Y. Wu, and W. Jia, "Beam tracking for UAV mounted SatCom on-the-move with massive antenna array," *IEEE J. Sel. Areas Commun.*, vol. 36, no. 2, pp. 363–375, Feb. 2018. doi: 10.1109/JSAC.2018.2804239.

[6] J. Zhao, F. Gao, G. Ding, T. Zhang, W. Jia, and A. Nallanathan, "Integrating communications and control for UAV systems: Opportunities and challenges," *IEEE Access*, vol. 6, pp. 67519–67527, Nov. 2018. doi: 10.1109/ACCESS.2018.2879637.

[7] E. W. Frew and T. X. Brown, "Airborne communication networks for small unmanned aircraft systems," *Proc. IEEE*, vol. 96, no. 12, pp. 2008–2027, Dec. 2008. doi: 10.1109/JPROC.2008.2006127.

[8] P. Zhan, K. Yu, and A. L. Swindlehurst, "Wireless relay communications with unmanned aerial vehicles: Performance and optimization," *IEEE Trans. Aerosp. Electron. Syst.*, vol. 47, no. 3, pp. 2068–2085, Jul. 2011. doi: 10.1109/TAES.2011.5937283.

[9] C. Dixon and E. W. Frew, "Optimizing cascaded chains of unmanned aircraft acting as communication relays," *IEEE J. Sel. Areas Commun.*, vol. 30, no. 5, pp. 883–898, Jun. 2012. doi: 10.1109/JSAC.2012.120605.

[10] Y. Zeng, R. Zhang, and T. J. Lim, "Throughput maximization for UAV-enabled mobile relaying systems," *IEEE Trans. Commun.*, vol. 64, no. 12, pp. 4983–4996, Dec. 2016. doi: 10.1109/TCOMM.2016.2611512.

[11] J. Chen, J. Xie, Y. Gu, S. Li, S. Fu, Y. Wan, and K. Lu, "Long-range and broadband aerial communication using directional antennas (ACDA): Design and implementation," *IEEE Trans. Veh. Technol.*, vol. 66, no. 12, pp. 10793–10805, Dec. 2017. doi: 10.1109/TVT.2017.2723802.

[12] J. M. I. Alonso and M. S. Pérez, "Phased array for UAV communications at 5.5 GHz," *IEEE Antennas Wireless Propag. Lett.*, vol. 14, pp. 771–774, Dec. 2014, 10.1109/LAWP.2014.2379442.

[13] S. Jenvey, J. Gustafsson, and F. Henriksson, "A portable monopulse tracking antenna for UAV communications," in *Proc. Int. Unmanned Air Veh. Syst. Conf.*, Bristol, U.K., Apr. 2007, pp. 1–7.

[14] C. She, C. Liu, T. Q. S. Quek, C. Yang, and Y. Li, "Ultra-reliable and low-latency communications in unmanned aerial vehicle communication systems," *IEEE Trans. Commun.*, vol. 67, no. 5, pp. 3768–3781, May 2019. doi: 10.1109/TCOMM.2019.2896184.

[15] H. C. Nguyen, R. Amorim, J. Wigard, I. Z. Kovács, T. B. Sørensen, and P. E. Mogensen, "How to ensure reliable connectivity for aerial vehicles over cellular networks," *IEEE Access*, vol. 6, pp. 12304–12317, 2018. doi: 10.1109/ACCESS.2018.2808998.

[16] V. Jaeck, L. Bernard, K. Mahdjoubi, R. Sauleau, S. Collardey, P. Pouliguen, and P. Potier, "A switched-beam conformal array with a 3-D beam forming capability in C-band," *IEEE Trans. Antennas Propag.*, vol. 65, no. 6, pp. 2950–2957, Jun. 2017. doi: 10.1109/TAP.2017.2696418.

[17] P. Sanchez-Olivares, P. P. Sanchez-Dancausa, and J. L. Masa-Campos, "Circularly conformal patch array antenna with omnidirectional or electronically switched directive beam," *IET Microw. Antennas Propag.*, vol. 11, no. 15, pp. 2253–2259, Dec. 2017. doi: 10.1049/iet-map.2017.0195.

[18] D. W. Matolak and R. Sun, "Unmanned aircraft systems: Air-ground channel characterization for future applications," *IEEE Veh. Technol. Mag.*, vol. 10, no. 2, pp. 79–85, Jun. 2015. doi: 10.1109/MVT.2015.2411191.

[19] Italiana Ponti Radio (IPR) S.R.L. *D-ATKS Command and Control (C2) Data Link Series*. Accessed: May 3, 2019. [Online]. Available: http://web.ipreurope.com/products/d-atks-command-control-c2-data-link-series/

[20] Italiana Ponti Radio (IPR) S.R.L. *HD Compact Video Downlink*. Accessed: May 3, 2019. [Online]. Available: http://web.ipreurope.com/products/hd-compact-video-downlink/

[21] X. Sun, R. Blázquez-García, A. García-Tejero, J. M. Fernández-González, M. Burgos-García, and M. Sierra-Castañer, "Circular array antenna tor UAV-UAV communications," in *Proc. 11th Eur. Conf. Antennas Propag.*, Paris, France, Mar. 2017, pp. 2025–2028.

[22] R. Garg, P. Barthia, I. Bahl, and A. Ittipiboom, *Microstrip Antenna Design Handbook*. Norwood, MA, USA: Artech House, 2001.

[23] *Digital Video Broadcasting (DVB); Framing Structure, Channel Coding and Modulation for Digital Terrestrial Television (DVB-T)*, document DVB A012, 2015.

[24] Y. Zeng, R. Zhang, and T. J. Lim, "Wireless communications with unmanned aerial vehicles: Opportunities and challenges," *IEEE Commun. Mag.*, vol. 54, no. 5, pp. 36–42, May 2016. doi: 10.1109/MCOM.2016.7470933.
[25] R. Prasad, *OFDM for Wireless Communications Systems*. Norwood, MA, USA: Artech House, 2004.
[26] *Propagation Curves for Aeronautical Mobile and Radionavigation Services Using the VHF, UHF and SHF Bands*, document Rec. ITU-R P.528-3, 2012.
[27] *Defining Propagation Model for Recommendation ITU-R P.528-3*, document ITU-R P2345-0, 2015.
[28] C. Pan, H. Ren, Y. Deng, M. Elkashlan, and A. Nallanathan, "Joint blocklength and location optimization for URLLC-enabled UAV relay systems," *IEEE Commun. Lett.*, vol. 23, no. 3, pp. 498–501, Mar. 2019. doi: 10.1109/LCOMM.2019.2894696.

RODRIGO BLÁZQUEZ-GARCÍA (S'17) was born in Madrid, Spain, in 1992. He received the B.Sc. and M.Sc. degrees in telecommunications engineering from the Universidad Politécnica de Madrid (UPM), Spain, in 2014 and 2016, respectively, where he is currently pursuing the Ph.D. degree with the Microwave and Radar Research Group, Department of Signals, Systems, and Radiocommunications, as a recipient of a scholarship from the Spanish Ministry of Education. His research interests include the area of radio frequency and radar systems, including signal and data processing techniques, and the design of microwave circuits.

XIAOLIANG SUN was born in Shanghai, China. He received the B.Sc. degree in telecommunications engineering and the M.Sc. degree in signal theory and communications from the Universidad Politécnica de Madrid (UPM), Madrid, Spain, in 2016 and 2018, respectively. He is currently pursuing the Ph.D. degree in communications technologies and systems with UPM. Since 2016, he has been with the Radiation Group, Department of Signals, Systems, and Radiocommunications, UPM. His research interests include phased array antennas, smart antennas, and beam-forming networks in millimeter band.

MATEO BURGOS-GARCÍA received the telecommunications engineering and Ph.D. degrees from the Universidad Politécnica de Madrid, Madrid, Spain, in 1989 and 1994, respectively. Since September 1988, he has been with the Microwave and Radar Research Group, Department of Signals, Systems, and Radiocommunications, Universidad Politécnica de Madrid, Madrid, Spain, where he is a Full Professor. His research interests include broadband digital receivers for spectrum surveillance and software-defined radios, broadband radars for low probability of interception and high-resolution applications, millimeter-wave radars, and synthetic aperture radar signal processing.

ALEJANDRO GARCÍA-TEJERO was born in Madrid, Spain. He received the B.Sc. and M.Sc. degrees in telecommunications engineering from the Universidad Politécnica de Madrid, Spain, in 2016 and 2018. In 2017, he joined the École Fédérale de Lausanne, Lausanne, Switzerland as Guest M.Sc. Student. He is currently working as RF/Antenna Engineer with Huber+Suhner AG, Switzerland. His research interests include RF circuits, communication and automotive radar antennas.

JUAN VIDAL-ALEGRÍA was born in Bilbao, Spain, in 1994. He received the B.Sc. and M.Sc. degrees in telecommunications engineering from the Universidad Politécnica de Madrid, in 2016 and 2018, respectively, and the M.Sc. degree in wireless communications from Lund University, in 2018. He is currently pursuing the Ph.D. degree with the Department of Electrical and Information Technology, Lund University. His main research interests include wireless communications, signal processing, and multiple antenna systems.

JOSÉ-MANUEL FERNÁNDEZ-GONZÁLEZ (SM'19) was born in Lausanne, Switzerland. He received the Diplôme d'Ingénieur en Électricité degree from the École Polytechnique Fédérale de Lausanne, Lausanne, in 2003, and the Ph.D. degree from the Universidad Politécnica de Madrid, Madrid, Spain, in 2009. In 2006, he joined the Centre de Recherches Poly-Grames, l'École Polytechnique de Montréal, Montreal, QC, Canada, and in 2007, he joined the Chalmers University of Technology, Göteborg, Sweden, as a Guest Ph.D. Student. Since 2013, he has been an Assistant Professor with the Universidad Politécnica de Madrid. In 2018, he was a Fulbright Visiting Researcher with Antenna Research Group, University of Colorado at Boulder. He has authored more than 90 publications in scientific journals, symposium proceedings and seminars, and he holds four patents. He has participated in more than 35 research projects and contracts. His research interests include phased array antennas, RF circuits, and metamaterial structures with emphasis on planar antenna applications.

MANUEL SIERRA-CASTAÑER (S'95–M'01–SM'12) was born in 1970 in Zaragoza, Spain. He received the telecommunications engineering and the Ph.D. degrees from the Universidad Politécnica de Madrid, Spain, in 1994 and 2000, respectively. He worked for the cellular company Airtel from 1995 to 1997. Since 1997, he has been with the University "Alfonso X"as Assistant, and since 1998 with Technical University of Madrid as Research Assistant, Assistant, Associate Professor, and Full Professor. His current research interests include planar antennas and antenna measurement systems. He received the IEEE APS 2007 Schelkunoff Prize Paper Award for the paper "Dual-Polarization Dual-Coverage Reflectarray for Space Applications" in 2007. He is the member of the Board of Director of European Association of Antennas and Propagation since 2016 and AMTA Europe Liaison since 2015.